AIP | Journal of Applied Physics

Thermal vibration characteristics of armchair boron-nitride nanotubes

Anirban Chandra, Puneet Kumar Patra, and Baidurya Bhattacharya

Citation: Journal of Applied Physics **118**, 234503 (2015); doi: 10.1063/1.4937559
View online: http://dx.doi.org/10.1063/1.4937559
View Table of Contents: http://scitation.aip.org/content/aip/journal/jap/118/23?ver=pdfcov
Published by the AIP Publishing

Thermal vibration characteristics of armchair boron-nitride nanotubes

Anirban Chandra,[1] Puneet Kumar Patra,[2] and Baidurya Bhattacharya[3,a)]
[1]Department of Mechanical Engineering, Indian Institute of Technology Kharagpur, Kharagpur 721302, India
[2]Advanced Technology Development Center, Indian Institute of Technology Kharagpur, Kharagpur 721302, India
[3]Department of Civil Engineering, Indian Institute of Technology Kharagpur, Kharagpur 721302, India

(Received 29 August 2015; accepted 29 November 2015; published online 16 December 2015)

A nanomechanical resonator based sensor works by detecting small changes in the natural frequency of the device in presence of external agents. In this study, we address the length and the temperature-dependent sensitivity of precompressed armchair Boron-Nitride nanotubes towards their use as sensors. The vibrational data, obtained using molecular dynamics simulations, are analyzed for frequency content through the fast Fourier transformation. As the temperature of the system rises, the vibrational spectrum becomes noisy, and the modal frequencies show a red-shift irrespective of the length of the nanotube, suggesting that the nanotube based sensors calibrated at a particular temperature may not function desirably at other temperatures. Temperature-induced noise becomes increasingly pronounced with the decrease in the length of the nanotube. For the shorter nanotube at higher temperatures, we observe multiple closely spaced peaks near the natural frequency, that create a masking effect and reduce the sensitivity of detection. However, longer nanotubes do not show these spurious frequencies, and are considerably more sensitive than the shorter ones. © *2015 AIP Publishing LLC*. [http://dx.doi.org/10.1063/1.4937559]

I. INTRODUCTION

Boron-Nitride nanotubes (BNNTs) have excellent mechanical properties[1,2] along with good chemical and thermal stability.[3,4] As a result, like their carbon counterpart, BNNTs have seen several applications, like protective shields for nanomaterials,[5] hydrogen storage,[6,7] sorption of gases,[8] water purification,[9] and fabrication of new composite materials.[10] The continuously shrinking size of nanomechanical devices, however, presents a problem; heat generated in these devices needs to be dissipated over *a small length*.[11] The resulting thermal induced vibrations may significantly hamper the desired performance of these devices. Interestingly, the vibrational frequencies can also be used to calculate the Young's modulus of the nanotubes.[12]

The temperature of the system significantly alters the mechanical behavior of the devices as well. Thus, understanding the structural response of the nanotubes under mechanical and thermal loads is important to realize their full potential. For example, applications, such as mass detection through nanomechanical resonators[13] rely predominantly on detecting the changes in the *natural* frequency of the nanotubes as the mass attaches itself to the latter. In fact, other sensing applications of nanomechanical resonators[14,15] also rely upon their dynamic characteristics. However, these mechanisms of detection assume that the vibrations induced by thermal loading, which is inherent in any nanomechanical device, does not alter the frequency spectrum drastically. Thus, the addition of significant noise, because of thermal loading, may wash out the small changes arising in the frequency spectrum, rendering it impractical to use nanomechanical resonators as detectors for use in highly sensitive cases.

Although the mechanical properties of Boron Nitride nanotubes have been studied for several years using molecular mechanics,[16] molecular dynamics simulations,[17] first principle studies,[18,19] and continuum modelling,[20,21] no such study exists for understanding the thermal induced vibrations, and their impact on device performance. The present study aims to address this gap. We employ molecular dynamics simulations to obtain the vibration data of armchair Boron-Nitride nanotubes of different lengths. To mimic the loading conditions seen in real applications,[22] we impose a precompression on the nanotubes. The resulting vibrational data are then analyzed for their frequency content. We show that the amplitude of the thermal induced noise is comparable to the amplitude of the mechanically induced vibrational frequencies for shorter length nanotubes, and the former have a masking effect on the latter, rendering the shorter nanotubes less sensitive towards sensing applications. However, for longer nanotubes, the noise induced in the frequency spectra due to thermal vibrations are much smaller.

II. MODELING AND SIMULATION

A. Boron Nitride Nanotubes

A Boron-Nitride sheet has hexagonal rings, where every atom of Nitrogen is covalently bonded to three different Boron atoms, and vice versa. The nearest BN bond length is $a = 1.4457$ Å.[23] Typically, three parameters: the chiral indices (n, m) and the length l are sufficient to characterize a BNNT. A chiral BNNT is denoted by a value of m that satisfies $0 < m < n$. A value of $m = 0$ gives us a zig-zag BNNT, while a value $m = n$ gives an armchair BNNT. In the present study, we restrict ourselves to the armchair (10, 10) BNNTs of two different lengths, 6.9 and 20.7 nm. The BNNTs have

a)Electronic mail: baidurya@civil.iitkgp.ernet.in.

been modelled using the nanotube builder tool of the open-source VMD package.[24]

B. Interaction potential

In the present study, we have adopted the three-body Tersoff-type potential[25] for modelling the interactions between the B-N atoms. The Tersoff potential can be expressed in the following form:

$$E = \sum_i E_i = \frac{1}{2}\sum_{i\neq j}\sum_j \phi(r_{ij})$$
$$\phi(r_{ij}) = \sum_i \sum_{j>1} f_c(r_{ij})\left[f_R(r_{ij}) + b_{ij} f_A(r_{ij})\right], \quad (1)$$

where r_{ij} is the distance between the ith and the jth atoms, b_{ij} represents the bond order function, f_C is the cutoff function that ensures the nearest-neighbor interaction, f_R represents the repulsive pair potential, and f_A is the attractive pair potential. The mathematical forms of the individual functions are as follows:

$$f_C(r_{ij}) = \begin{cases} 1 & \forall r_{ij} < R_{ij} \\ \frac{1}{2} - \frac{1}{2}\sin\left(\frac{\pi}{2} \times \frac{r_{ij} - R_{ij}}{S_{ij} - R_{ij}}\right) & \forall R_{ij} < r_{ij} < S_{ij} \\ 0 & r_{ij} > S_{ij} \end{cases}$$
$$f_R(r_{ij}) = Ae^{-\lambda_1 r_{ij}}, \quad f_A(r_{ij}) = -Be^{-\lambda_2 r_{ij}},$$
$$b_{ij} = \left(1 + \beta^n \zeta_{ij}^n\right)^{-\frac{1}{2n}},$$
$$\zeta_{ij} = \sum_{k\neq i,j} f_C(r_{ik}) g(\theta_{ijk}) \exp\left[\lambda_3^3 (r_{ij} - r_{ik})^3\right],$$
$$g(\theta_{ijk}) = 1 + c^2/d^2 - c^2/\left[d^2 + (h - \cos\theta_{ijk})^2\right], \quad (2)$$

where θ_{ijk} represents the angle between the bonds $i - j$ and $i - k$. Depending upon the system being simulated, the parameters in the equation take different values. For BN materials, several Tersoff potential parameters have been proposed.[26,27] In the present study the parameters proposed by Sevik *et al.*,[28] which was obtained by fitting the simulation results to the structural, mechanical, and vibrational characteristics of hexagonal BN, have been used. We were motivated to use this potential parameter set because of its widespread use[25,29] and good agreement with results from first principle studies and experiments.[28,30]

C. Simulation mechanism

In this work, we have tried to keep the boundary conditions, and the external environment as close to real-life experiments as possible. Typically, in experiments that involve nanomechanical resonators, the nanotubes are connected between two electrodes, the "source" and the "drain."[31–34] A small part of the nanotube, along each end, rests on these electrodes, and the adhesion between the two surfaces provides clamping at the suspension points. Thus, a good choice of modelling these nanotube resonators is by treating the boundaries as clamped-clamped.[35] Because of the source-drain configuration, a tensile/compressive stress is induced in the nanotube.[22] The effect of tensile and compressive stresses on the sensitivity of nanoresonator performance has been well studied.[31,36] An effective way of introducing tensile and compressive stresses in the nanotubes is by prestretching/precompressing them prior to clamping.

Molecular dynamics simulation is performed using the open source LAMMPS package.[37] The entire nanotube is divided into three regions, 1, 2, and 3 as shown in Figure 1(a). The second region has 3 rings, 1, 2, and 3. Regions 1 and 3, and all the rings are 5 Å in length. Each ring is comprised of four layers of atoms. In this study, the z coordinate is along the axis of the nanotube, whereas the x and y coordinates specify the transverse directions.

At the beginning of the simulation, region 3 of the BNNT is fixed, as shown in Figure 1(b), and the resulting structure is minimized using conjugate gradient to obtain a stable configuration. During the minimization procedure, region 1 of the BNNT is allowed to move freely only in the z direction (along the axis) to prevent any spurious nanotube bending, while region 2 is kept free from any constraints.

Subsequently, the system is subjected to a uniaxial compression by imposing a constant displacement rate of 0.1 Å/*fs* on region 1 along the negative z direction, as shown in Figure 1(c), until a strain of 0.725% is reached. Thus, the shorter nanotube (of 6.9 nm length) is compressed by 0.5 Å and the longer nanotube (of 20.7 nm length) is compressed by 1.5 Å. Each compression step (of 0.1 Å/*fs*) is followed by 5000 equilibration steps performed at near ground state of 0.1 K using the Nosé-Hoover thermostat.[38] The time step for performing the numerical integration is 1 fs. Post-achieving the desired compression, region 1 is also kept fixed, as shown in Figure 1(d), such that the nanotube now has a clamped-clamped boundary condition.

Since we are interested in thermal vibrations, it is imperative that the temperature be increased from 0.1 K. The

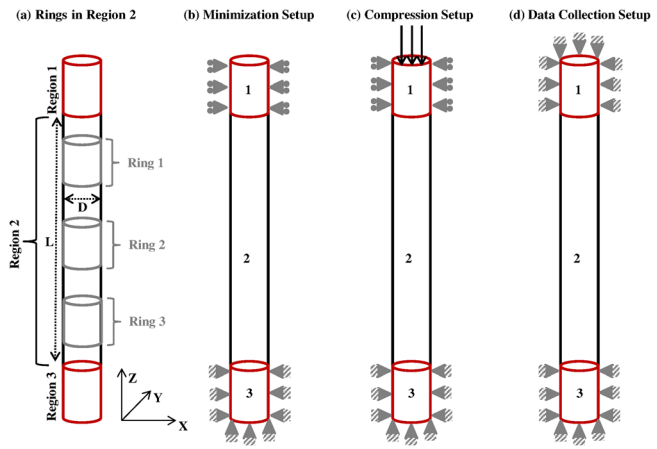

FIG. 1. (a) Division of a nanotube into regions and rings. Each BNNT has three regions, 1, 2, and 3. Certain subsections of region 2 that have a length of 5 Å are labelled as rings. (b) Setup during minimization. The bottom region marked 3 is kept fixed in all directions. The top region marked 1 is allowed to move only along the z direction. The region marked 2 is allowed to move freely. (c) The nanotube is compressed along the negative z direction. (d) Post the desired compression is achieved, the region 1 is kept fixed along all three directions.

fluctuations in the instantaneous temperature arise due to the Nosé-Hoover thermostat and serve as the input noise. It can be shown from theoretical arguments that the fluctuations decrease with an increase in system size.[39] We slowly ramp the temperature to the desired value at 0.05 K per fs. Once the system reaches the desired temperature, 200 000 NVT equilibration runs are performed. The relevant vibration data are collected for these 200 000 time steps, and is then further analyzed. We limit ourselves to analyzing the center of mass displacements of the three rings shown in Figure 1. For each ring, we calculate the center of mass displacement along the x and y directions as follows:

$$x_{com} = \frac{1}{N}\sum_{i}^{N}(x_i); \quad y_{com} = \frac{1}{N}\sum_{i}^{N}(y_i), \tag{3}$$

where the summation is carried over the N atoms that constitute the ring. The resulting center of the mass data are then analyzed for the frequency content by performing a fast Fourier transform in MATLAB. We discuss our findings next.

III. RESULTS AND DISCUSSIONS

The coupled nature of the Nosé-Hoover equations of motion solved in the simulations makes it difficult to separate the thermal effects from pure mechanical vibration. The thermostat variable of the equations of motion is directly influenced by the temperature of the system. The temporal evolution of the thermostat variable, in turn, modifies the momentum evolution equation. Thus, there is an interesting interplay between the temperature and the response variables. However, it is *important* to know the mechanical frequencies in the absence of the thermal excitations for gauging the noise induced by the thermal loading. In order to accomplish this, we perform a set of simulations under constant particle number, volume and energy (NVE) conditions, postequilibrating the system at 0.1 K. The particles comprising the second ring have been imposed with small velocities (5 Å/ps) along the x and y directions. The data collected, as a result, is Fourier transformed to obtain the vibrational frequencies, as shown in Figure 2. For a particular nanotube, in the absence of thermal excitations, the vibrational spectra along the x and y directions are almost overlapping. There are uniquely defined sharp peaks in the power spectra corresponding to the different modes of vibration.

Let us now look at the frequency spectra dependence on temperature for the two nanotubes, the first one being 6.9 nm long and the second one being 20.7 nm long. The input noise (i.e., the coefficient of variation) is 2.7% for the shorter nanotube, and 1.5% for the longer nanotube. In typical experimental realizations of nanomechanical resonators, the response is usually measured at the center of the nanotube suspended between the source-drain electrode.[32] Therefore, to make our results consistent with the experimental setups, the first set of results, shown in Figure 3, correspond to the second ring (see Figure 1). Moreover, the amplitude of vibrations of ring 2 are observed to be the largest among the three rings, providing yet another reason to analyze the second ring first.

Figure 3 shows the power spectra along the x direction for the two nanotubes at three different temperatures. The inset figures show a zoomed-in view near the first modal vibration frequency at a temperature of 1000 K. A comparison with Figure 2 shows that the noise due to thermal excitations are in the range of the modal frequencies obtained due to mechanical vibrations. As the temperature increases, the peaks in the shorter BNNT get dispersed and thus it becomes difficult to exactly pinpoint the natural frequencies. The frequency spectra of the shorter nanotube also shows that these closely spaced multiple frequencies are practically indistinguishable, and have high amplitudes associated with them. The presence of closely spaced frequencies renders it difficult to use the shorter nanotubes in highly sensitive mass detection or any other application that depends on the changing frequency content. This is because the change in frequency content due to the external agent may get "masked" by these closely-spaced nearby multiple frequencies. In essence, the nanotube can work as a sensor only if the external agent is large enough to overcome the thermal noise, i.e., the sensitivity of the instrument decreases. The power spectra for y_{com} show similar features as well. Similar closely spaced frequencies around the natural frequencies are observed for the other rings as well for the shorter nanotube (see Figure 4).

On the one hand, in the longer BNNT (see Figure 3 (right)), specific natural modes of vibration still prevail at higher temperatures, and there is no evidence of multiple frequencies of *high amplitude* around any modal frequency, making the longer nanotube based devices ideal for sensitive sensing applications. The amplitudes of vibrations of both the BNNTs are seen to increase as the temperature is increased, which is not very surprising.

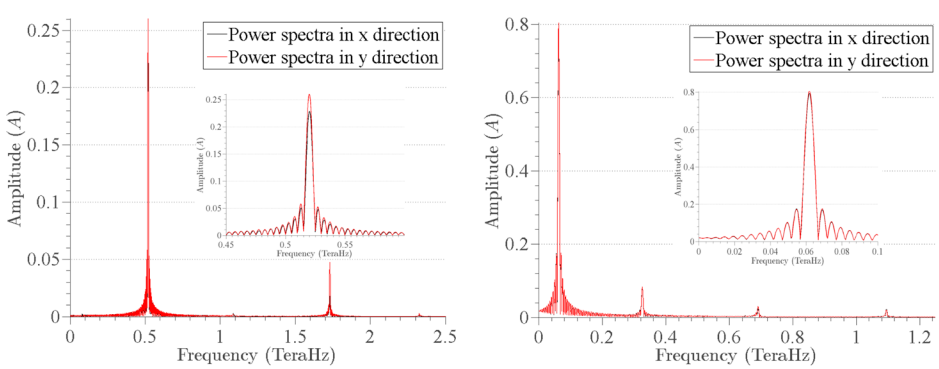

FIG. 2. Power spectra for ring 2 solely due to mechanical vibrations for (left) 6.9 nm nanotube, and (right) 20.7 nm nanotube. The x and y vibrational spectra are nearly the same for both cases. The inset figures show a zoomed-in view near the first mode of vibration.

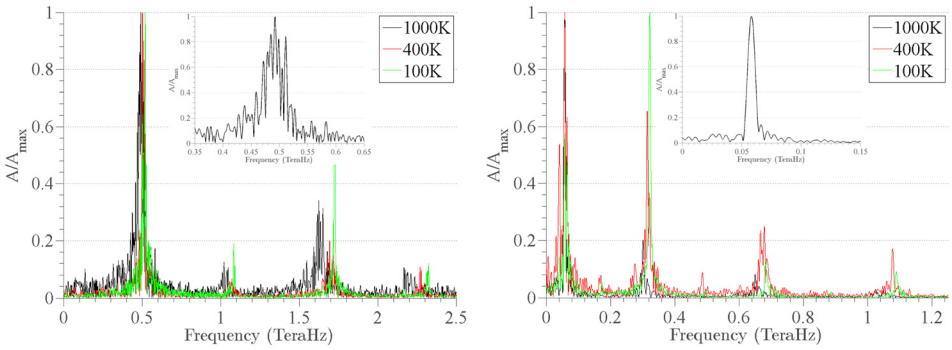

FIG. 3. Power spectra for ring 2 at different temperatures: (left) 6.9 nm long BNNT, and (right) 20.7 nm long BNNT. The inset figures show a zoomed-in view near the first modal vibration frequency. For the shorter nanotube, it is clear from the inset figure, that at higher temperature, multiple frequencies with high amplitudes get excited. This unwanted feature is absent in the longer nanotube. These results correspond to x_{com}. A similar conclusion can be drawn for y_{com} as well.

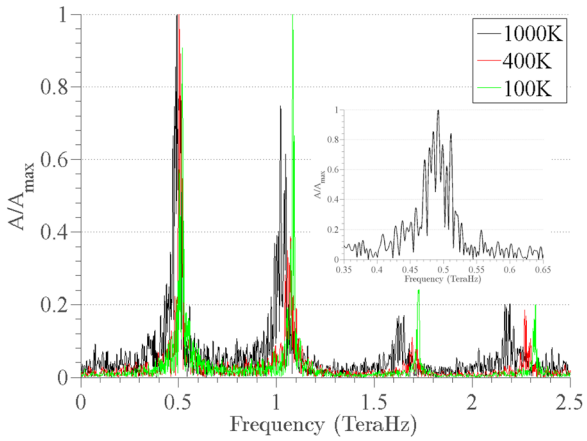

FIG. 4. Power spectra for ring 1 along the x direction at different temperatures for the 6.9 nm nanotube. The inset figure shows the presence of multiple closely-spaced high-amplitude frequencies near the first vibration frequency.

Another repercussion of the presence of multiple frequencies near the fundamental mode for the shorter nanotube is our inability to reconstruct the dynamics from the modal data. Given the power spectrum data, with distinct k natural frequencies (ω_1 to ω_k), the dynamics can be reconstructed using the following expression:

$$x_{com,r}(t) = \sum_{i=1}^{k} A_i \sin(\omega_i t + \phi_i) + c. \tag{4}$$

Here, ϕ_i is the phase of the ith frequency, and c is a constant that is obtained from the power spectra at zero frequency. A reconstruction of the dynamics of ring 2, based on the first four modes for both nanotubes, is shown in Figure 5. Despite significant efforts, we could not exactly pinpoint some of the modal frequencies (due to thermal noise) for the shorter nanotube, and hence have taken the largest amplitude frequencies from amongst the multiple closely-spaced frequencies. It is evident that the actual dynamics could be reconstructed using the first four modes for the longer nanotube, while for the shorter nanotube, no meaningful result can be obtained using the modal data.

Let us now look at the change in the frequency spectra arising due to an increase in temperature. It is important to note that at low temperatures the natural frequencies obtained does not change with the ring considered, but their relative contributions might change. At higher temperatures while in one ring it may be impossible to single out the modal frequencies (see the inset Figure 3(left)), in the other rings it might not be difficult to do so. In general, it is seen that in the rings closer to the fixed regions, thermal vibrations are not so pronounced and better estimates of the natural frequencies may be obtained. We reiterate that some of the previous figures have been plotted for the second ring, keeping in mind that in real spectrometry and experiments, measurements are usually taken at the center of the nanotube. We plot the first four frequencies corresponding to the vibration of ring 1, which lies closer to the boundary (see Figure 1). The results are shown in Figure 6. In typical structural mechanics or continuum models of nanotubes, successive frequencies vary as the square of the mode number. However, a comparison based on Figure 6 shows that such does not hold true for our case.

The length of the nanotube greatly influences the natural frequencies of vibration and their contributions. The modal frequencies of the shorter BNNT are significantly higher as compared to the longer BNNT. As the temperature increases,

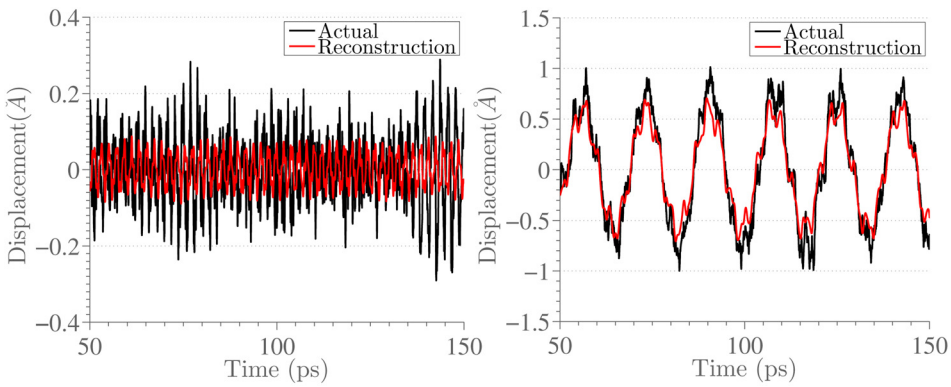

FIG. 5. Reconstructing the actual dynamics of the second ring through modal contributions at 1000 K: (left) 6.9 nm long BNNT constructed using the first four modes, and (right) 20.7 nm long BNNT constructed using the first four modes. Notice that the first four modes are able to provide a good description of the actual dynamics for the longer nanotube. For the shorter nanotube on the other hand, no meaningful result can be extracted from the reconstructed dynamics.

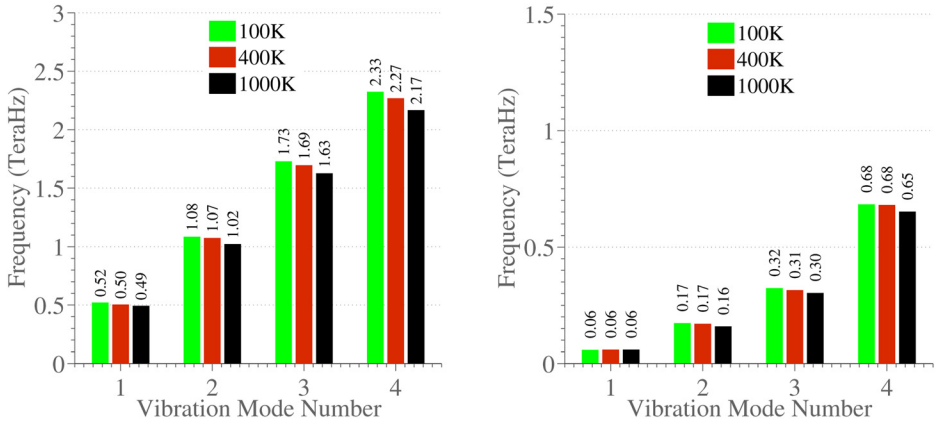

FIG. 6. The first four modal frequencies for x_{com} of the first ring at different temperatures for the: (left) 6.9 nm long BNNT, and (right) 20.7 nm long BNNT. The frequencies show a red-shift (i.e., they decrease), which is more pronounced for the shorter nanotube and higher modes.

the first four modal frequencies show a red-shift. This shift is more pronounced for (i) the shorter nanotube than the longer nanotube, and (ii) the higher modes than the fundamental mode. The results highlight two important points: (i) a nanomechanical oscillator device calibrated at a given temperature cannot be used directly for highly sensitive sensing applications without recalibration, and (ii) nanomechanical oscillator devices based on shorter nanotubes are more susceptible to thermal fluctuations than the longer ones. Our limited exploration with chiral and zig-zag nanotubes reveal that similar conclusions could be drawn about them as well, however, at larger precompressing strains. The red-shift of the frequency spectrum is reminiscent of the damped harmonic oscillator, where the frequency at which the peak amplitude occurs, decreases with increasing damping coefficient. Drawing a parallel, we conjecture that in the present case, the Nosé-Hoover reservoir variable (which acts *like* the damping coefficient) is responsible for the shift in frequency.

IV. CONCLUSIONS

Throughout this work, we highlight the importance of the thermal environment and the length of the nanotubes for nanomechanical devices that rely on change in natural frequency for sensing applications. Our results indicate that as the devices become smaller, the thermal effects become pronounced, so much so that they can mask the additional contribution arising due to an external factor. The masking effect *may* result in decreasing sensitivity of the devices with increasing temperature. Apart from inducing a "noise" in the frequency spectrum, a higher system temperature also causes a red-shift of the frequency spectrum, i.e., the modal frequencies decrease with increasing temperature. Thus, the devices calibrated at a certain temperature may not perform desirably at higher temperatures.

[1]J. Garel, I. Leven, C. Zhi, K. Nagapriya, R. Popovitz-Biro, D. Golberg, Y. Bando, O. Hod, and E. Joselevich, Nano Letters **12**, 6347 (2012).
[2]M. Santosh, P. K. Maiti, and A. K. Sood, J. Nanosci. Nanotechnol. **9**, 5425 (2009).
[3]W.-Q. Han, W. Mickelson, J. Cumings, and A. Zettl, Appl. Phys. Lett. **81**, 1110 (2002).
[4]D. Golberg, Y. Bando, C. Tang, and C. Zhi, Adv. Mater. **19**, 2413 (2007).
[5]Y. Li, P. Dorozhkin, Y. Bando, and D. Golberg, Adv. Mater. **17**, 545 (2005).
[6]X. Wu, J. Yang, J. G. Hou, and Q. Zhu, J. Chem. Phys. **124**, 054706 (2006).
[7]R. Ma, Y. Bando, H. Zhu, T. Sato, C. Xu, and D. Wu, J. Am. Chem. Soc. **124**, 7672 (2002).
[8]M. D. Ganji, A. Mirnejad, and A. Najafi, Sci. Technol. Adv. Mater. **11**, 045001 (2010).
[9]W. Lei, D. Portehault, D. Liu, S. Qin, and Y. Chen, Nat. Commun. **4**, 1777 (2013).
[10]C. Zhi, Y. Bando, C. Tang, S. Honda, H. Kuwahara, and D. Golberg, J. Mater. Res. **21**, 2794 (2006).
[11]E. Pop, S. Sinha, and K. E. Goodson, Proc. IEEE **94**, 1587 (2006).
[12]N. G. Chopra and A. Zettl, Solid State Commun. **105**, 297 (1998).
[13]C. Li and T.-w. Chou, Appl. Phys. Lett. **84**, 5246 (2004).
[14]P. S. Waggoner and H. G. Craighead, Lab on a Chip **7**, 1238 (2007).
[15]X. Huang, M. Manolidis, S. C. Jun, and J. Hone, Appl. Phys. Lett. **86**, 143104 (2005).
[16]T. C. Theodosiou and D. A. Saravanos, Int. J. Comput. Methods Eng. Sci. Mech. **12**, 203 (2011).
[17]W. H. Moon and H. J. Hwang, Nanotechnol. **15**, 431 (2004).
[18]Y. Kinoshita and N. Ohno, Phys. Rev. B **82**, 085433 (2010).
[19]D. V. Fakhrabad and N. Shahtahmassebi, Mater. Chem. Phys. **138**, 963 (2013).
[20]E.-S. Oh, Mater. Lett. **64**, 859 (2010).
[21]J. Song, J. Wu, Y. Huang, and K. C. Hwang, Nanotechnol. **19**, 445705 (2008).
[22]K. Eom, H. S. Park, D. S. Yoon, and T. Kwon, Phys. Rep. **503**, 115 (2011).
[23]A. Rubio, J. L. Corkill, and M. L. Cohen, Phys. Rev. B **49**, 5081 (1994).
[24]W. Humphrey, A. Dalke, and K. Schulten, J. Mol. Graphics **14**, 33 (1996).
[25]J. Tersoff, Phys. Rev. B **39**, 5566 (1989).
[26]V. Verma, V. K. Jindal, and K. Dharamvir, Nanotechnol. **18**, 435711 (2007).
[27]W. Sekkal, B. Bouhafs, H. Aourag, and M. Certier, J. Phys.: Condens. Matter **10**, 4975 (1998).
[28]C. Sevik, A. Kinaci, J. B. Haskins, and T. Çağin, Phys. Rev. B **84**, 085409 (2011).
[29]N. M. Anoop Krishnan and D. Ghosh, J. Appl. Phys. **115**, 064303 (2014).
[30]A. Kinaci, J. B. Haskins, C. Sevik, and T. Çağin, Phys. Rev. B **86**, 115410 (2012).
[31]V. Sazonova, Y. Yaish, H. Ustunel, D. Roundy, T. A. Arias, and P. L. McEuen, Nature **431**, 284 (2004).
[32]B. Lassagne, D. Garcia-Sanchez, A. Aguasca, and A. Bachtold, Nano Lett. **8**, 3735 (2008).
[33]H.-Y. Chiu, P. Hung, H. W. C. Postma, and M. Bockrath, Nano Lett. **8**, 4342 (2008).
[34]H. B. Peng, C. W. Chang, S. Aloni, T. D. Yuzvinsky, and A. Zettl, Phys. Rev. Lett. **97**, 087203 (2006).
[35]C. Li and T.-W. Chou, Phys. Rev. B **68**, 073405 (2003).
[36]S. S. Verbridge, D. F. Shapiro, H. G. Craighead, and J. M. Parpia, Nano Lett. **7**, 1728 (2007).
[37]S. Plimpton, J. Comput. Phys. **117**, 1 (1995).
[38]W. G. Hoover, Phys. Rev. A **31**, 1695 (1985).
[39]K. Huang, *Introduction to Statistical Physics* (CRC Press, 2009).